THE JOURNAL OF PHYSICAL CHEMISTRY B
A JOURNAL OF THE AMERICAN CHEMICAL SOCIETY

pubs.acs.org/JPCB

Article

Native Function of the Bacterial Ion Channel SthK in a Sparsely Tethered Lipid Bilayer Membrane Architecture

Published as part of The Journal of Physical Chemistry virtual special issue "Steven G. Boxer Festschrift".

Jakob Andersson,[□] David Kleinheinz,[□] Ulrich Ramach, Nikolaus Kiesenhofer, Alex Ashenden, Markus Valtiner, Stephen Holt, Ingo Koeper, Philipp A. M. Schmidpeter,* and Wolfgang Knoll*

Cite This: *J. Phys. Chem. B* 2023, 127, 3641−3650

Read Online

ACCESS | Metrics & More | Article Recommendations | Supporting Information

ABSTRACT: The plasma membrane protects the interiors of cells from their surroundings and also plays a critical role in communication, sensing, and nutrient import. As a result, the cell membrane and its constituents are among the most important drug targets. Studying the cell membrane and the processes it facilitates is therefore crucial, but it is a highly complex environment that is difficult to access experimentally. Various model membrane systems have been developed to provide an environment in which membrane proteins can be studied in isolation. Among them, tethered bilayer lipid membranes (tBLMs) are a promising model system providing a solvent-free membrane environment which can be prepared by self-assembly, is resistant to mechanical disturbances and has a high electrical resistance. tBLMs are therefore uniquely suitable to study ion channels and charge transport processes. However, ion channels are often large, complex, multimeric structures and their function requires a particular lipid environment. In this paper, we show that SthK, a bacterial cyclic nucleotide gated (CNG) ion channel that is strongly dependent on the surrounding lipid composition, functions normally when embedded into a sparsely tethered lipid bilayer. As SthK has been very well characterized in terms of structure and function, it is well-suited to demonstrate the utility of tethered membrane systems. A model membrane system suitable for studying CNG ion channels would be useful, as this type of ion channel performs a wide range of physiological functions in bacteria, plants, and mammals and is therefore of fundamental scientific interest as well as being highly relevant to medicine.

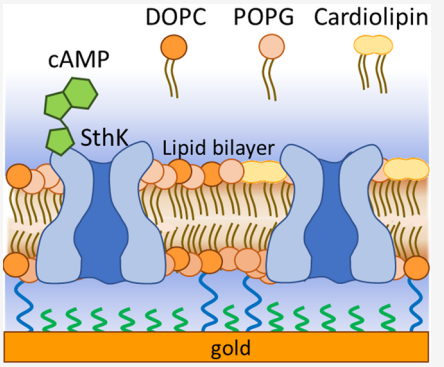

INTRODUCTION

Besides serving as a barrier protecting the cellular interior from outside influences, the plasma membrane is also an essential interface between the cell and its surroundings, exchanging signals with other cells, importing nutrients, and exporting signaling molecules and waste products. Due to the myriad roles it fulfils, the cell membrane and its components are among the most important drug targets, with approximately two-thirds of existing pharmaceuticals targeting components of the cell membrane.[1] Ion channels in particular are critical to facilitate cell−cell communication to regulate physiological activity and often play a role in conditions such as epilepsy[2] and other neurological conditions,[3] cancer,[4,5] and viral infections.[6] It is therefore crucial to study membrane proteins and the processes they facilitate. However, the cell membrane is a highly complex environment with limited experimental accessibility.

Studying ion channels is particularly challenging and while it is possible to do so via patch clamp electrophysiology, the technique requires substantial skill and training and typically has low throughput. Moreover, as the experiment takes place in the cellular membrane, the method suffers from interference from other membrane components and allows no direct control over membrane composition. Various model membrane systems have been developed, most notably the free-standing bimolecular lipid membranes (BLMs),[7] which achieve excellent electrical resistance but are fragile and also limited in terms of applicable experimental techniques. Bilayer stability can be improved by depositing the membrane on a solid support, creating supported lipid bilayers (SLBs), which significantly expands the range of applicable analytical tools.[8] While it is possible to form high-resistance SLBs,[9] they remain comparatively susceptible to mechanical disturbances and, depending on the bilayer formation protocol, can contain a high number of defects, making them less suitable to study ion channels.[10] Moreover, while the inner leaflet of solid-supported membranes is lubricated by a 10−20 Å water layer, this may

Received: October 15, 2022
Revised: March 28, 2023
Published: April 18, 2023

https://doi.org/10.1021/acs.jpcb.2c07252
J. Phys. Chem. B 2023, 127, 3641−3650

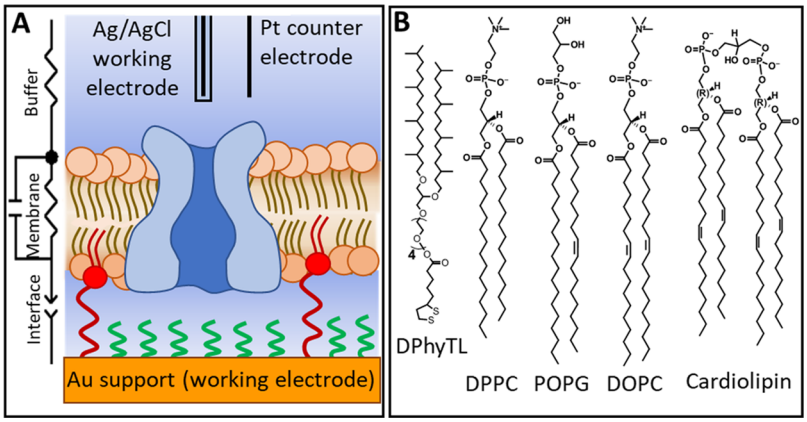

Figure 1. (A) Schematic of a sparsely tethered lipid bilayer on a gold support comprised of DPhyTL (red) mixed with mercaptoethanol (green) as a spacer molecule, electrode arrangement and equivalent circuit used to fit EIS data, if not stated otherwise. (B) Structures of DPhyTL and the phospholipids used to form the lipid bilayers.

not prevent embedded proteins from contacting the support, which could affect their structure and function, particularly in case of ion channels which must undergo conformational changes for gating.[11]

To improve the stability of the membrane and reduce interactions of the membrane with the supporting material, the inner leaflet can be suspended above the supporting material using a short hydrophilic spacer such as ethylene glycol. This reduces interactions between the support and the lipid bilayer while also significantly increasing its robustness and electrical resistance. The membrane architecture we have used is based on DPhyTL (Figure 1B) which enables the formation of bilayers that remain intact for up to 9 months[12] and can achieve resistances in the GΩ-range.[13] When the inner leaflet is comprised exclusively of DPhyTL, the bilayer is densely packed and contains very little water in the submembrane region.[14] While these membrane systems have high electrical resistance and allow for incorporation of pore-forming peptides[15,16] and bacterial toxins such as alpha hemolysin,[17] gramicidin[18] and cytolysin,[19] they are not well-suited for the incorporation of membrane proteins as they do not have sufficient fluidity to accommodate them and only limited space under the membrane allows for ion transport.

Submembrane hydration can be improved by diluting the anchorlipid with a spacer molecule such as mercaptoethanol,[20] allowing the reconstitution of ion channels such as the insect odorant receptor coreceptor.[21] DPhyTL-based membrane architectures have also been used to study the effect of silver nanoparticles on lipid bilayers[22] and to study the function of antibiotics[23] as well as the combination of membrane-targeting antibiotics and nanoparticles.[24] Here we use a sparsely tethered lipid bilayer membrane (stBLM, Figure 1A) to reconstitute the SthK ion channel.

SthK is a cyclic nucleotide-gated (CNG) ion channel found in *Spirochaeta thermophila*.[25] CNG channels are nonselective cation channels activated by cyclic adenosine or guanosine monophosphate (cAMP or cGMP) and are found in eukaryotes for example in sensory neurons[26] as well as in prokaryotes. SthK is very well characterized functionally[25,27,28] and structurally[29,30] and thus represents an ideal model to evaluate the applicability of stBLMs for functional studies of membrane proteins. Furthermore, the function of SthK is dependent on the lipid composition of the membrane.[31] This makes it an ideal protein to demonstrate the utility of tethered membrane systems to study ion channels whose function depends on more complex lipid mixtures. A model membrane environment allowing native function of CNG ion channels would offer an environment where the effects of mutations, phosphorylation, and drug candidates can be investigated under robust, controlled conditions. Moreover, it would allow the replication of complete mammalian signaling pathways, for example, olfaction, offering a unique opportunity to study disorders caused by mutations in the protein machinery facilitating these pathways.

As it has been shown that SthK activity is highly dependent on membrane composition,[25] we used three different lipid compositions to study its function (see Table 1): pure 1,2-dipalmitoyl-*sn*-glycero-3-phosphocholine (DPPC) in which receptor function is impeded, DPPC supplemented with cardiolipin (CL), in which some receptor function is possible, and a 1,2-dioleoyl-*sn*-glycero-3-phosphocholine 1-palmitoyl-2-oleoyl-*sn*-glycero-3-phospho-glycerol CL mixture, which has been shown to allow optimal ion channel function.

Table 1. Lipid Components in Different Membrane Compositions (Ratios in Molar Percentage)

bilayer composition	DPPC (%)	CL (%)	DOPC (%)	POPG (%)
DPPC	100			
DPPC-CL	50	50		
DOPC-POPG-CL		20	50	30

MATERIALS AND METHODS

Chemicals. Milli-Q-grade water (18.2 MΩ cm resistance) was produced using an arium pro system and used to prepare all buffer solutions. Ultrapure ethanol (99.9% purity, water free) was purchased from Merck and used to prepare all anchorlipid solutions and to clean substrates. Phospholipids were purchased from Avanti Polar Lipids. All other chemicals were purchased from Merck or VWR and used without further purifications. Silicon substrates for template-stripping were purchased from Crystec and Si-Mat. DPhyTL was synthesized by Celestial Synthetics (https://www.celestialsynthetics.com).

Preparation of Template-Stripped Gold (TSG). Gold surfaces were prepared via template stripping, as described previously.[21,32] Polished silicon wafers were sonicated in acetone to remove residues from the polishing procedure,

https://doi.org/10.1021/acs.jpcb.2c07252
J. Phys. Chem. B 2023, 127, 3641−3650

followed by cleaning with acidic piranha solution (3:1 sulfuric acid and a 33% hydrogen peroxide in water) for 60 min, and then rinsed thoroughly with ultrapure water and ethanol, followed by drying in a nitrogen stream.

Gold Deposition. A film thickness of 50 nm gold (99.99% supplied by MaTeck) was deposited by evaporation at a rate of 0.1 Å/s. (6 A current, 10^{-6} mbar). Borosilicate glass microscopy slides were then glued to the exposed gold surface using EPO-TEK354 optical adhesive mixed at a 10:1 ratio of monomer/curing agent which was stirred thoroughly for 5 min and degassed under vacuum at 60 °C for 1 h before use. The adhesive was deposited at 120 °C for 10 min and cured for 3 h at 160 °C.

SthK Expression and Purification. SthK ion channel protein was expressed in *E. coli* C41 (DE3) cells (Lucigen) as previously described.[25,30] Briefly, cells were grown in LB media at 37 °C in baffled flasks. At an OD_{600} of 0.4 cells were transferred to 20 °C and further grown to an OD_{600} of 0.9, at which protein expression was induced overnight by the addition of a final concentration of 0.5 mM IPTG. Cells were harvested (10 min, 4000 × g, 4 °C) and resuspended in breaking buffer (50 mM Tris, pH 7.8, at room temperature; 100 mM KCl; and 200 μM cAMP, supplemented with PMSF (85 μg/mL), leupeptin/pepstatin (0.95/1.4 μg/mL), DNaseI (1 mg; MilliporeSigma), lysozyme (1 mg; MilliporeSigma), and cOmplete ULTRA mini protease inhibitor (Roche)). The entire purification was carried out at 4 °C. First, cells were broken by sonication (Sonic Dismembrator 500, Thermo Fisher Scientific), and membranes were solubilized by the addition of 30 mM *n*-dodecyl-β-D-maltopyranoside (DDM; Anatrace). Protein extraction was performed for 90 min under gentle agitation. Insoluble components and cell debris were pelleted by centrifugation (37500 × g, 45 min, 4 °C), the supernatant was filtered (0.22 μm membrane) and applied to a 5-ml HiTrap chelating HP Co^{2+} column (GE Healthcare Life Sciences) preequilibrated in wash buffer (20 mM HEPES, pH 7.8, 100 mM KCl, 30 mM imidazole, 200 μM cAMP, and 0.5 mM DDM). Unbound proteins were removed by washing with 15 column volumes of wash buffer and SthK protein was eluted by washing with 15 mL of wash buffer supplemented with 300 mM imidazole. The eluate was concentrated to 10 mg/mL (Amicon ultra concentrator, MilliporeSigma) with a 100 kDa cutoff and loaded onto a Superdex 200 10/300 GL gel filtration column (GE Healthcare Life Sciences) pre-equilibrated in 20 mM HEPES, pH 7.4, 100 mM KCl, and 0.5 mM DDM.

Reconstitution of SthK into Small Unilamellar Vesicles. Right after gel filtration, SthK was reconstituted into liposomes for impedance measurements. This reconstitution was performed at room temperature. 1,2-Dioleoyl-*sn*-glycero-3-phosphocholine (DOPC), 1-palmitoyl-2-oleoyl-*sn*-glycero-3-phospho-(1′-rac-glycerol) (POPG), and 18:1 cardiolipin or 1,2-dipalmitoyl-*sn*-glycero-3-phosphocholine (DPPC) and 18:1 cardiolipin (all lipids from Avanti Polar Lipids) were mixed in chloroform in ratios of 5:3:2 or 1:1, respectively, and dried under a constant N_2 stream. Lipids were resolubilized in *n*-pentane, dried again under a N_2 stream, and resolubilized in reconstitution buffer (10 mM HEPES, 400 mM KCl, and 5 mM NMG [*N*-methylglucamine gluconate], pH 7.6) in the presence of 33 mM CHAPS (3-((3-cholamidopropyl) dimethylammonio)-1-propanesulfonate, Anatrace). SthK in DDM was added to the solubilized lipids (5 μg SthK per mg lipid) and incubated for 10 min to allow for efficient formation of lipid-detergent mixed micelles. Liposome formation was performed by detergent removal. 500 μL of the protein−lipid mixtures were loaded onto an 18 mL detergent removal column (Sephadex G-50 fine beads, GE Healthcare Life Sciences) and eluted with reconstitution buffer. For each lipid composition liposome containing fractions were identified by visual inspection for turbidity, pooled, aliquoted, and flash frozen in liquid N_2. Proteo-liposomes were stored at −80 °C.

SAM Preparation. Freshly cleaved TSG slides were rinsed thoroughly with ultrapure ethanol and dried under a stream of nitrogen before immersion in an ethanolic solution with a combined concentration of 0.1 mM comprised of 20% DPhyTL and 80% mercaptoethanol. Substrates were functionalized at 4 °C overnight and then removed from the solution, rinsed thoroughly with ultrapure ethanol, dried under a stream of nitrogen, and immediately used for bilayer formation.

Bilayer Formation. SthK-containing liposomes (5 or 100 μg protein/mg lipid) were prepared immediately prior to bilayer formation by extrusion (31×) through track-etched polycarbonate membranes (50 nm pores) using the Avanti mini-extruder kit. Ten μL of liposome solution were then immediately added to the substrate with 50 μL of 138 mM PBS solution and incubated for 18 h at 30 °C. The membrane was then rinsed slowly with 5 cell volumes (5 mL) of 138 mM PBS solution and monitored for stability via EIS over a period of 2 h to ensure their electrical properties did not deteriorate before commencing the experiment.

Atomic Force Microscopy. AFM measurements were conducted using a Cypher ES (Oxford Instruments, United Kingdom) on a vibration isolated table. The measurements were done in 1x PBS under ambient pressure and temperature. In this setup an ARROW-UHFAuD gold-coated silicon cantilever (NanoWorld AG, Switzerland) with resonance frequencies between 700 and 2000 kHz was used. Operation of the AFM was conducted through blueDrive technology in tapping mode (TM-AFM) with scan rates between 2 and 8 Hz. Data were analyzed using the Gwyddion software package (http://gwyddion.net/).

Neutron Scattering Experimental. All neutron experiments were performed at the Australian Nuclear Science and Technology Organization (ANSTO) at the 20 MW OPAL reactor (Lucas Heights, Sydney, Australia). Neutron reflectometry (NR) measurements were conducted using the PLATYPUS time-of-flight neutron reflectometer.[29] Cold neutrons with wavelengths from 2.5 to 18 Å were used. The reflected intensity of the neutrons was measured at glancing angles of 0.5°, 0.9°, and 5° under D_2O, H_2O, and CM4.5 (a mixture of 76% D_2O and 24% H_2O). All measurements were completed in 100 mM $CaCl_2$, unless otherwise stated, for approximately 2 h per contrast. Preparation of the substrates was conducted at the South Australian node of the ANFF. Briefly, 10 cm diameter by 1 cm thickness polished circular crystal silicon disks were cleaned using a 1:1:5 mixture of NH_3/H_2O_2/Milli-Q for 1 h at 70 °C. They were then rinsed with ultrapure water and ethanol (Sigma-Aldrich, Australia) and dried with nitrogen. The substrates were then coated with 5 nm chromium (100 mA current) and 20 nm gold (10 mA) via sputter coating. Monolayers and bilayers were formed as described for the EIS experiments.

For neutron scattering, three different bilayers were produced. The first bilayer was pretreated with 100 μL of cationic nanoparticles for 18 h, rinsed and then 10 mg/mL colistin were added. The second bilayer was exposed for 18 h

https://doi.org/10.1021/acs.jpcb.2c07252
J. Phys. Chem. B 2023, 127, 3641−3650

to a mixture of 100 μL of nanoparticles and 10 mg/mL colistin sulfate. The third bilayer was exposed to 1 mL AuNP for 18 h, rinsed and then exposed to colistin sulfate for an additional 18 h.

Data Analysis. Neutron data were fitted to a multilayer model (see Figure 2A). Each layer is fitted with a thickness, a roughness (with respect to the preceding layer), a scattering length density, and a hydration level (in volume %). Data was fitted using the Python-based Refnx program.[30] Data were fitted using a differential evolution algorithm using 100 iterations. Parameters were set to the expected values for each layer and allowed to vary within a reasonable range. The model used to fit the data was a slab-based model used previously.[6]

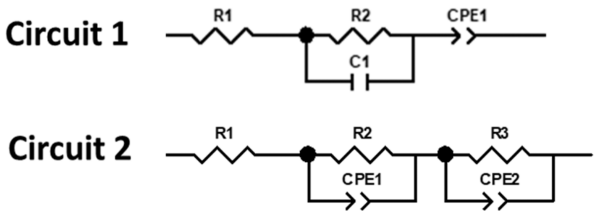

Figure 2. Equivalent electrical circuits used to fit EIS data. R1: electrolyte resistance, R2: membrane resistance, R3: submembrane reservoir/spacer resistance, C1: membrane capacitance, CPE2: gold interface/submembrane reservoir capacitance.

Electrochemical Impedance Spectroscopy (EIS). EIS measurements were performed using a dual channel Metrohm Autolab potentiostat with a three-electrode (gold working electrode, Ag/AgCl reference electrode and Pt wire counter electrode). The counter electrode was placed at a maximum distance of 1 cm from the working electrode. A total of 20−30 frequencies were measured between 100 kHz and 5 mHz (10 mV amplitude) in 1× PBS buffer solution. Data were analyzed using ZView2 (Scribner Associates) by fitting the measured impedance data to one of two equivalent electrical circuits (see Figure 2). CPE1 in circuit 1 represents the imperfect capacitance of the Helmholtz capacitance of the gold interface modified by the presence of the inner membrane leaflet. In circuit 2, CPE1 represents a capacitor that has become imperfect due to conductive pathways between the capacitor plates enabled by ion channel opening. CPE1 in circuit 1 and CPE2 in circuit 2 are necessary to achieve a good fit with low error values on other circuit elements, but if the value is fitted, it typically associated with an error exceeding 100%, because the EIS spectrum contains insufficient data points in the low frequency range (<10 mHz) for an accurate fit. We therefore do not allow the parameters to vary during the fitting process. In circuit 1, CPE1 always had a fixed value of $Q = 2 \times 10^{-4}$ Fcm^{-2} $s\alpha^{-1}$ ($\alpha = 0.8$). When circuit 2 was used, a second CPE element was required to reproduce the phase angle below 90° upon ligand addition. If this was the case, the parameters for CPE1 can be fitted with a low error and the value is reported in Table 2. Instead, when using circuit 2, the second CPE has a fixed value of 2×10^{-4} μFcm^{-2} $s\alpha^{-1}$ ($\alpha = 0.9$). R2 for circuit 2 was always fixed with a resistance of 10^8 Ω cm^2, as it too cannot be fitted with the existing data but was necessary to obtain a good fit to the experimental data. Recording additional data points below 5 mHz is unfeasible, as it requires 20 min of measurement time or more per data point, and the measurements are prone to errors from interference by external electrical fields, even when inside a Faraday cage. All spectra were area-normalized using a surface area of 0.28 cm^2. The errors of the fitting values are reported as the range of values which can be fitted without decreasing the quality of the fit based on least-squares fitting.

RESULTS AND DISCUSSION

Bilayer formation was tested using liposomes containing either 5 or 100 μg protein per mg lipid. Successful bilayer formation was only possible using the lower concentration of protein, but the reason for this is unclear. It is possible that at higher protein content, vesicle fusion was no longer thermodynamically favorable, and liposomes adsorbed to the substrate without fusing. While it was possible to form sealing lipid bilayers using all membrane compositions, SthK function was observed only in bilayers containing cardiolipin (Figure 5).

Bilayer Formation and Topological Characterization of SthK-tBLMs. To first confirm bilayer formation, we imaged membranes with atomic force microscopy (AFM). Prior to bilayer formation, the gold surface (functionalized with the DPhyTL/mercaptoethanol-SAM) has an ghness of 1.6 nm.[21] After bilayer formation, SthK-tBLMs had a roughness of 0.28−0.35 nm (Figure 3A), which is in good agreement with previously reported properties of lipid bilayers.[33] AFM images of SthK-stBLMs showed features with a height of 3−4 nm (6 nm when examined with slower scanning speed (Figure 3C). This corresponds well to the dimensions reported for the cytosolic cyclic nucleotide binding domain (CNBD) and the C-linker domain of SthK,[34] demonstrating that lipid bilayers formed successfully and that SthK was embedded in an orientation (with CNBD regions facing the solvent) that allows for functional studies. We also observed a single pinhole defect with a depth of approximately 4 nm, corresponding to the thickness of the lipid bilayer (Figure 3A).

At higher resolution, AFM is able to resolve a single ion channel (Figure 3C), and the apparent dimensions are in agreement with cryo-EM studies. The height of about 6 nm, corresponds well to the C-linker/CNBD domains of SthK.[25] The lateral dimensions of around 20 nm, however, are larger than the tetrameric channel assembly, which can be explained

Table 2. Structural Parameters of SthK-tBLMs Comprised of the DOPC-POPG-CL Lipid Mixture[a]

	thickness (Å)	SLD (10^{-6} $Å^{-2}$)	hydration (vol %)	roughness (Å)
tether region	8.27 ± 0.31	0.67 ± 0.29	20.61 ± 0.62	2.18 ± 0.13
inner head groups	4.16 ± 0.23	1.03 ± 0.04	28.81 ± 1.25	3.27 ± 0.26
inner hydrocarbon chains	8.5 ± 0.2	−0.24 ± 0.01	3.67 ± 0.75	8.74 ± 0.88
outer hydrocarbon chains	8.5 ± 0.2	−0.24 ± 0.01	1.98 ± 1.02	3.46 ± 0.92
outer head groups	11.2 ± 1.03	1.55 ± 0.07	64.2 ± 1.13	7.86 ± 0.28

[a]The full set of fitting data, including parameters for the substrate structure, as well as an additional set of neutron data, can be found in the Supporting Information, Table S2.

https://doi.org/10.1021/acs.jpcb.2c07252
J. Phys. Chem. B 2023, 127, 3641−3650

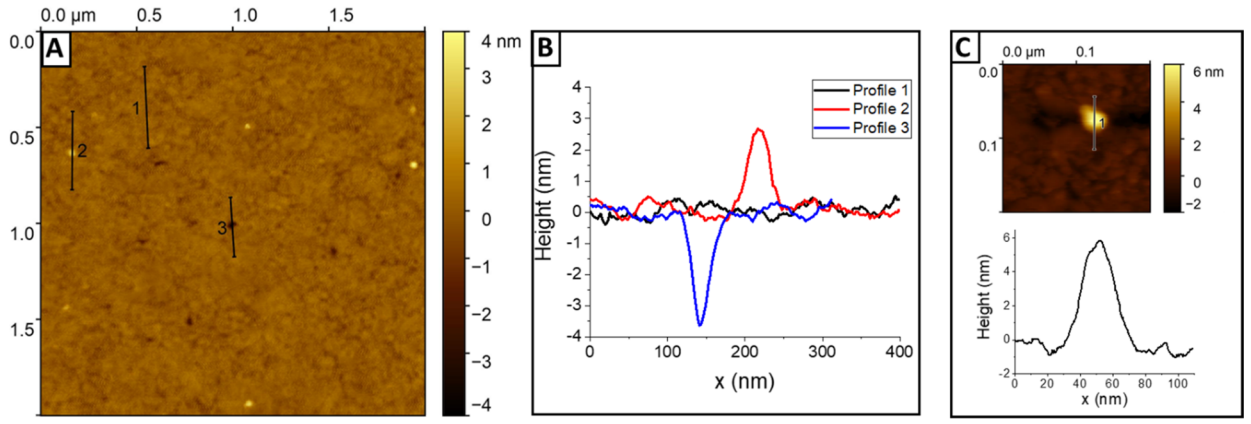

Figure 3. (A) 2 × 2 μm AFM image of an stBLM comprised of the DOPC-POPG-CL lipid mixture containing several SthK ion channels. (B) Height profiles: profile 1 is the membrane only and profiles 2 and 3 cross an ion channel and a defect, respectively. (C) AFM image of a single SthK ion channel (top) and height profile of the ion channel (bottom). Additional AFM data are shown in the Supporting Information in Figure S2.

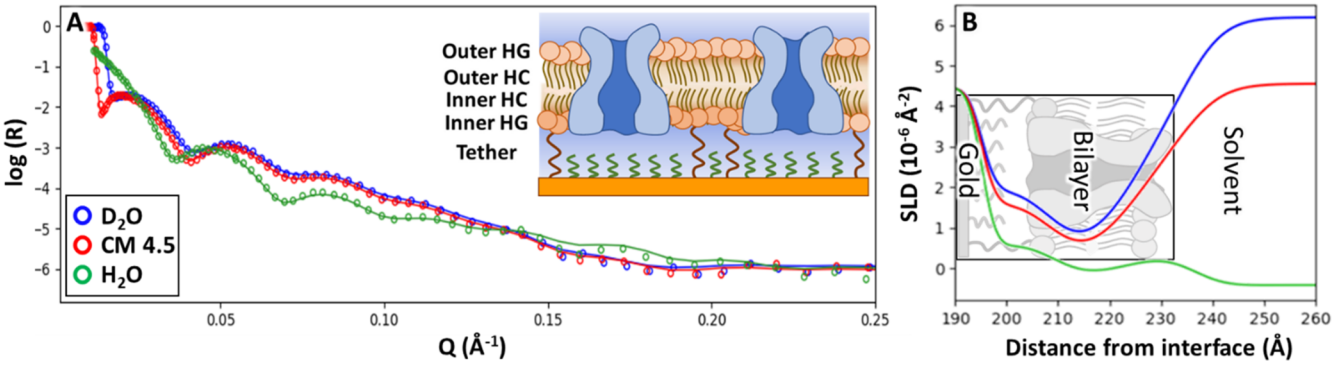

Figure 4. (A) Neutron scattering plot of SthK-stBLM comprised of the DOPC-POPG-CL lipid mixture (open symbols are experimental data, lines represent the fits) and (B) fitted SLD profile. The inset shows the approximate change of the SLD profile across the membrane. An additional data set is shown in the Supporting Information, Figure S3.

by the shape of the AFM tip. A sharper AFM cantilever with higher stiffness may provide a better image but also carries the risk of damaging or deforming the protein and the lipid bilayer.[35] We could not observe changes in membrane topology upon addition of cAMP, presumably because conformational changes in SthK are too subtle to be resolved by the AFM setup used here. The ion channel density varied considerably across the sample, with areas of lower density such as that shown in Figure 3A and significantly higher density (see Figure S2C in the Supporting Information).

Structural Characterization of SthK-tBLMs. To further confirm lipid bilayer formation, we characterized the membrane architectures with neutron scattering, a technique which enables the examination of buried soft matter interfaces in aqueous solution. Due to the restricted availability of beam time at neutron scattering facilities, we only measured samples with the lipid mixture which facilitated best ion channel function (DOPC-POPG-CL). To determine the structure of SthK-stBLMs, bilayers were prepared on polished 4″ silicon wafers via vesicle fusion and characterized in D_2O or H_2O and a mixture of the two with a scattering length density (SLD) matching gold (CM 4.5).

The data was fitted using the Refnx program.[36] Several methods have been developed to analyze neutron data including using space-filling models assuming a continuous distribution of membrane components,[37] or by dividing the lipid bilayer into a series of slabs. We used a slab-based model (Figure 4A) to allow easy comparison to previous studies of tethered and sparsely tethered membrane systems.[14,20,23,24] Each slab is assigned a distinct thickness, roughness (with respect to the preceding layer), hydration (in volume-%) and SLD (in units of 10^{-6} Å^{-2}). The SLD for each slab (or membrane section) is the average scattering length density of all atoms in the given volume.

The change in SLD of each layer upon exchanging solvents indicates the amount of water contained within each layer (Figure 4B).[20] Large variations with contrast changes are expected in the tether region as well as inner and outer head groups, as they contain significant amounts of water. Only minimal changes are expected in the inner and outer hydrocarbon chains as low-defect membranes contain 2% water or less in the hydrocarbon chain segment. The parameters extracted from fitting the neutron data are listed in Table 2. The thickness of the tether region is lower than that of membranes with an inner leaflet comprised of 100% DPhyTL (approximately 2 nm[14]). An additional layer is needed in sparsely tethered membranes to account for the inner headgroups of phospholipids incorporated into the lower leaflet,[20] the thickness of which would normally also be attributed to the tether segment. At 20%, the hydration of the tether region is typical for sparsely tethered membranes. The hydration of the inner head groups is higher than protein-free stBLMs,[20] but the inner headgroup region also contains proteins.

https://doi.org/10.1021/acs.jpcb.2c07252
J. Phys. Chem. B 2023, 127, 3641−3650

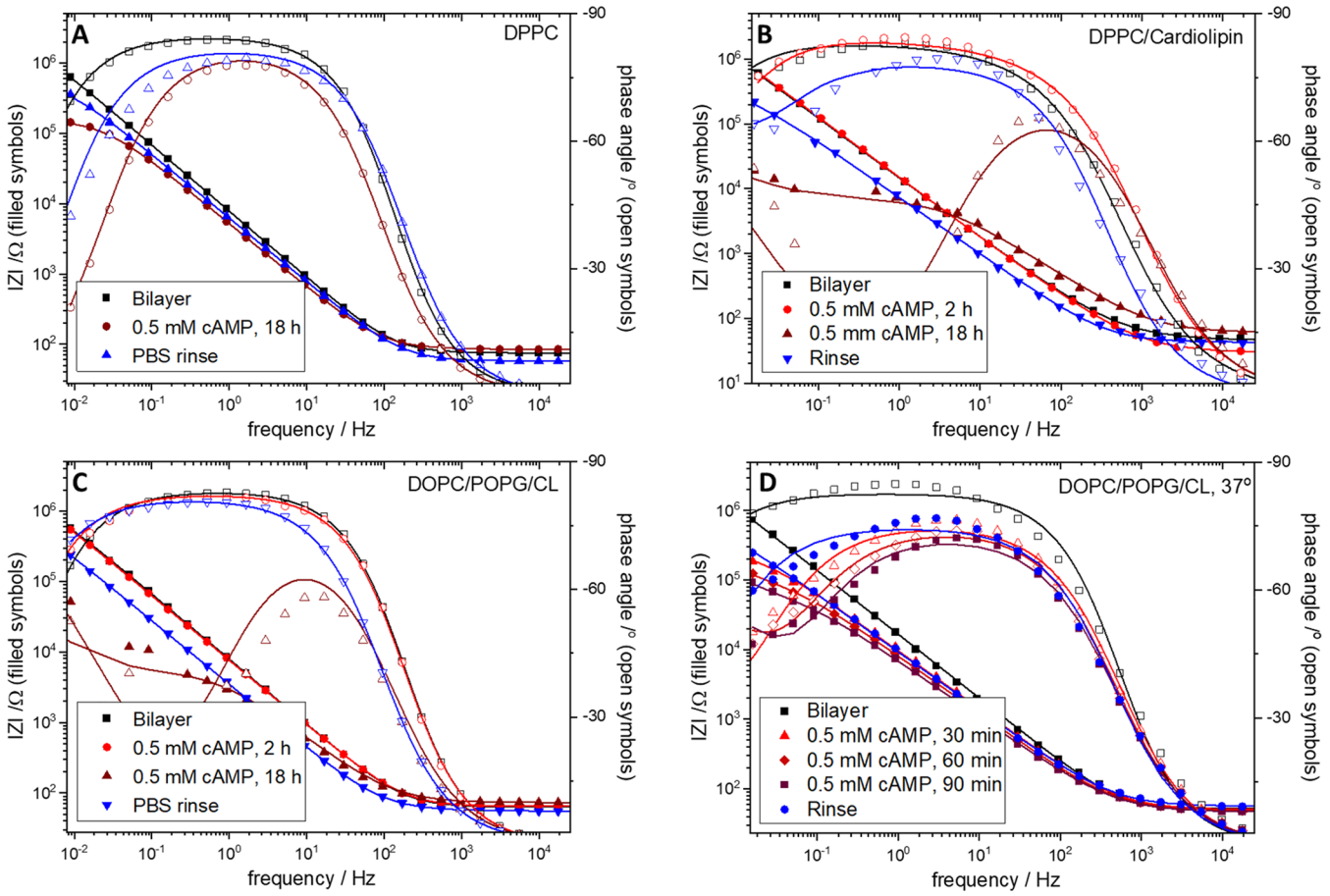

Figure 5. (A) Cyclic AMP response to SthK embedded a membrane comprised of DPPC only. (B) Cyclic AMP response to SthK embedded in a DPPC/CL membrane. (C) Cyclic AMP response to SthK embedded in a DOPC/POPG/CL membrane architecture. (D) Faster response of an SthK ion channel to the ligand at 37 °C.

Due to their composition, proteins typically have an SLD of $2-3 \times 10^{-6}$ Å^{-2}, the SLD varies with the amount of protons exchanged with the solvent,[38] which can take place even when the ion channel is embedded in lipid bilayers.[39] Therefore, some of the change in SLD of the inner head groups, hydrocarbon chains and outer head groups of the membrane is due to SLD change of the protein rather than water.

The protein content of the membranes can be estimated by comparing the SLD and the hydrocarbon segment in protein-free stBLMs (-0.4×10^{-6} Å^{-2})[14,20] to that of SthK-stBLMs (between -0.1 and -0.2×10^{-6} Å^{-2}). As the total SLD of a slab is the sum of the SLDs of the individual components, $x \times \mathrm{SLD}_{\mathrm{bilayer}} + y \times \mathrm{SLD}_{\mathrm{protein}} = -0.2-0.2 \times 10^{-6}$ Å^{-2}, where x and y are the volume fractions of the lipid bilayer and protein, respectively, leading to an estimated protein content of the membrane of 5−10%, depending on whether the SLD of the protein is assumed to be 2 or 3×10^{-6} Å^{-2}. However, as discussed earlier, membrane hydration is determined by the change in SLD upon change of the solvent contrast, as in protein-free lipid membranes, all SLD changes of the membrane can be attributed to the replacement of water molecules with D_2O. However, given that the SLD of proteins can also change with the solvent contrast,[39] it is likely that the fitting approach we used overestimates membrane hydration and underestimates protein content. The slab-model of tethered membranes is therefore not ideal to study heterogeneous protein-containing membranes. However, the primary objective of this work was to confirm the formation of SthK-stBLMs and compare their structure to protein-free stBLMs that are described using the slab-based model. For better structural characterization, an adjusted slab-based model or composition-space modeling approaches such as that used by Hoogerheide and colleagues is used for protein-containing supported membranes.[39]

Electrochemical Characterization of SthK-stBLMs. After confirming bilayer formation and structure, we used electrochemical impedance spectroscopy (EIS) to study the response of the ion channel to cAMP. EIS is one of the most commonly used techniques to study the dielectric properties of the tethered membrane system. The technique is highly sensitive to changes in membrane capacitance and resistance that occur upon ion channel opening. For a detailed discussion of the use of EIS to characterize tethered membranes, we recommend Valincius et al.[40]

After bilayer formation and before ligand addition, SthK-containing tethered membranes had resistances in the low MΩ cm^2 range, which is typical for DPhyTL-based tethered membranes.[20,41,42] Membrane capacitance was around 10−20 μF cm^{-2}, which is considerably higher than protein-free tethered membranes.[14,20] Increased capacitance of protein-containing tethered membranes has been reported previously, for example, in tethered membranes containing the insect odorant receptor coreceptor[21] or cytochrome C oxidase[43] and can be attributed to the higher dielectric constant of proteins,

https://doi.org/10.1021/acs.jpcb.2c07252
J. Phys. Chem. B 2023, 127, 3641−3650

especially ion channels that may contain water even in a closed state.[44] An estimate of the dielectric constant of SthK can be obtained from this data assuming a protein content of 10%, based on the neutron data.

As the total capacitance of the membrane is the sum of the capacitances of the individual components, and the dielectric constant ($\varepsilon_{bilayer}$) of a lipid bilayer is approximately 3,[45] and neutron data showing a thickness of the hydrocarbon chains (i.e., the dielectric material in the parallel place capacitor used to approximate the lipid bilayer) of ca. 2 nm (see Table 2), the lipid component of the membrane has a capacitance of ca. 1 μF/cm^2. The capacitance of the whole system (C_{total}) = $x \times C_{bilayer} + y \times C_{protein}$ = 10 μF/cm^2, where x and y represent the fractions of lipid bilayer and protein, respectively. Assuming a protein fraction of 0.1, $C_{protein}$ = 90 μF/cm^2. Approximating the lipid bilayer with a parallel place capacitor in which $C = \varepsilon_{dielectric} \times \varepsilon_0 \times A/d$, where $\varepsilon_{dielectric}$ is the permittivity of the dielectric material separating the parallel plate capacitors, ε_0 is the permittivity of free space, A is the area of the parallel plates, and d is the distance separating them, this leads to an estimate of $\varepsilon_{protein} \approx 200$, which is unrealistic. However, as discussed, the estimate of protein content from neutron scattering appears to be too low. Assuming a protein content of 20−25% instead leads to a dielectric constant of 60−85. Accounting for the errors in the various parameters that contribute to this assumption, this is in relatively good agreement with what has been suggested for the dielectric constant of ion channel pores.[46] Additional capacitance may also be contributed by charging of the cyclic nucleotide binding domain of SthK that extends above the lipid bilayer. Finally, the capacitance is estimated here based only on a relatively simple equivalent circuit comprised of a linear combination of resistors and capacitors. However, capacitors in electrolyte solutions do not adhere to these idealized assumptions in reality. For example, there appears to be a frequency-dependent element to capacitors in electrolyte solutions,[47] and frequency-dependent capacitance has been observed in the membranes of apical skin cells.[48] More complex model systems are therefore needed to better interpret EIS data of heterogeneous tethered membrane systems.

Ion channel opening is indicated by a significant reduction in membrane resistance between one[20] and four orders of magnitude.[17,21] However, as membrane resistance can also be reduced due to defect formation, we first determined the stability of the membrane system by measuring bilayer stability over time. We found no significant reductions in membrane resistance after 5 days (see Supporting Information, Figure S1) and reductions in membrane resistance can therefore confidently be attributed to ion channel function rather than defect formation. To activate SthK channels, we applied 0.5 mM cAMP, a concentration that leads to maximum SthK response.[25] To ensure cAMP does not affect protein-free membranes, we incubated a bilayer comprised of DPhyPC overnight with 1.5 mM cAMP (see Figure S1 and Table S1).

EIS data of the different membrane architectures before and after ligand addition are shown in the form of Bode plots (Figure 5). The electrical properties (resistance and capacitance) of the membranes can be extracted from EIS data by fitting it to an equivalent circuit comprised of a resistor approximating electrolyte resistance, a parallel resistor/capacitor describing the lipid bilayer and an additional constant phase element (CPE) accounting for the capacitance of the gold interface (Figure 2). A CPE represents an imperfect capacitor, accounting for the presence of conductive defects that allow leakage pathways between the capacitor plates and is very commonly used to fit impedance spectra of tethered membranes.[20,49−51] For a capacitor, the impedance (Z) depends on the frequency as follows:

$$Z = \frac{1}{C \times j \times \omega} \tag{1}$$

The CPE contains an additional parameter (α) This parameter can take on a value between 0 (a purely resistive element) and 1 (a purely capacitive element):

$$Z = \frac{1}{Q \times (j \times \omega)^{\alpha}} \tag{2}$$

Q is the CPE coefficient with units of μF cm^{-2} s$^{\alpha-1}$. In addition to being used for the submembrane region, which is a highly complex environment where the gold interface capacitance is modified by the presence of the SAM, a CPE is also used when a membrane contains conductive defects. These could be due to holes formed by a pore-forming toxin[52] and when the lipid bilayer contains ion channels to account for charge transport pathways facilitated by the protein.

The parameters extracted from fitting the EIS data are summarized in Table 3. When circuit 1 (see Figure 2) was used to fit experimental data, a CPE was required to obtain good fits of the experimental data. However, in circuit 1, CPE1 always had a fixed value of $Q = 2 \times 10^{-4}$ F cm^{-2} s$^{\alpha-1}$ (α = 0.8). Fixing the capacitance at this value was necessary to obtain a good fit for the high frequency segment of the data, but the value of the parameter cannot be interpreted in a meaningful way as there are insufficient experimental data points to allow fitting. Measuring below 5 mHz is not feasible, as the measurements requires a large amount of time (an hour or more per data point) and the signal at low frequencies is unstable and suffers from interference, rarely yielding useful data.

When circuit 2 was used, CPE1 can be fitted with a low error, and the value is reported in Table 2. When using circuit 2, the second CPE has a fixed value of 2×10^{-4} μF cm^{-2} s$^{\alpha-1}$ (α = 0.9) instead. R2 for circuit 2 was always fixed with a resistance of 10^8 Ω cm^2 as the parameter can also not be fitted properly but was necessary to obtain a good fit to the experimental data. Instead of using circuit 2, it would also be possible to fit the experimental data only to 100 mHz, where circuit 1 would be sufficient to obtain a good fit.

Sealing lipid bilayers could be formed, regardless of lipid composition, but in the absence of cardiolipin, only very small levels of ion channel activation were observed, as reported previously.[53] Upon cAMP addition, membrane resistance decreased by around 3 orders of magnitude in lipid bilayers containing CL. Along with a decrease in membrane resistance, the capacitance of the membrane increased by a factor of 2−4, which can be attributed to an increase in water content of the ion channels and to the population of the submembrane reservoir by ions as reported previously.[21] Alternatively, it is possible that upon ion channel opening, the membrane itself is no longer visible in EIS, and the data instead shows the capacitance of the monolayer and the submembrane space. However, a good fit required two capacitors in series, suggesting that there are still two distinct capacitive elements in the system, suggesting that the submembrane space and the gold interface have distinct capacitances.

https://doi.org/10.1021/acs.jpcb.2c07252
J. Phys. Chem. B 2023, 127, 3641−3650

Table 3. Electrical Properties of Different SthK-stBLMs upon Addition of cAMP Addition

Stability of SthK-stBLM in DOPC/POPG/CL				
	resistance ($M\Omega$ cm^2)	capacitance (μF cm^{-2})	Q of CPE1 (μF cm^{-2} $s^{\alpha-1}$)	circuit used to fit data
0 h	5.4 ± 1.8	19 ± 0.1		1
24 h	4.6 ± 2.5	19 ± 0.1		1
72 h	5.4 ± 0.4	20 ± 0.1		1
120 h	4.5 ± 0.3	22 ± 0.1		1
DPPC				
initial bilayer	2.3 ± 0.1	24 ± 0.1		1
500 μM cAMP, 18 h	0.22 ± 0.02		38 ± 0.3, α = 0.92	2
PBS flush	1.13 ± 0.02	27 ± 0.2		1
DPPC/CL				
initial bilayer	8.2 ± 0.9	12 ± 0.2		1
500 μM cAMP, 2 h	6.6 ± 0.6	12 ± 0.1		1
500 μM cAMP, 18 h	0.003 ± 0.0003		41 ± 5.5, α = 0.93	2
PBS flush	1.2 ± 0.1	38 ± 8.2		1
DOPC/POPG/CL				
initial bilayer	2.0 ± 0.9	25 ± 0.3		1
500 μM cAMP, 2 h	1.8 ± 0.2	26 ± 0.3		1
500 μM cAMP, 18 h	0.005 ± 0.0002		55 ± 2.7, α = 0.91	2
PBS flush	2.6 ± 0.3	52 ± 0.3		1
DOPC/POPG/CL, 37 °C				
initial bilayer	9.5 ± 2.9	11 ± 0.2		1
500 μM cAMP, 30 min	0.2 ± 0.1	25 ± 6.2		2
500 μM cAMP, 60 min	0.08 ± 0.02		35 ± 6.3, α = 0.96	1
500 μM cAMP, 90 min	0.04 ± 0.01		36 ± 6.3, α = 0.95	1
PBS flush	1.0 ± 0.1		23 ± 0.4, α = 0.95	1

At room temperature, ion channel response was relatively slow, requiring 12 hours or more to reach maximum channel opening, but increasing the temperature to 37 °C led to a significantly faster reduction in membrane resistance after 30–60 min. This may be explained by increased membrane fluidity at higher temperatures, as well as increased conformational flexibility of the ion channel. Moreover, given that the ion channel stems from *Spirochaeta thermophila*, an extremophile with optimal growth temperatures of approximately 68 degrees,[54] it is possible that it responds faster at higher temperatures. To ensure the reduction in membrane resistance was due to the opening of SthK by cAMP, we incubated SthK-tBLMs first with the partial agonist cyclic guanosine monophosphate which only results in minor ion channel activation at high concentrations.[30] We found only a small reduction in membrane resistance (approximately 5 $M\Omega$ cm^2) after 2 h and no further change in resistance upon addition of cAMP, showing that the bound cGMP effectively blocks cAMP activity. The Bode plots and data can be found in Figure S2 and Table S2, respectively.

By rinsing the membrane with PBS buffer, membrane resistance recovered to approximately the initial level or slightly lower, indicating ion channel closing upon ligand removal. However, a full recovery was not possible indicating that some ion channels remain open and membrane capacitance did not decrease upon ligand removal, suggesting that ions remained in the submembrane reservoir and that some ion channels remained open, possibly due to the presence of residual ligand molecules.

CONCLUSION

We present here a sparsely tethered lipid bilayer membrane architecture containing the functional SthK ion channel, showing that sparsely tethered membrane architectures can be prepared from complex lipid mixtures, that the environment required by the membrane system is sufficiently representative of native conditions and that ion channel function and lipid dependence are consistent with other electrophysiological experiments. We also showed that a comprehensive range of tools can be applied to tethered membranes, allowing electrochemical characterization by EIS, topological studies with AFM and structural studies with neutron scattering. In combination, this yields a comprehensive picture of membrane protein structure using an accessible platform prepared via self-assembly. Tethered membranes therefore offer an easy-to-use, self-assembled platform to study membrane protein function in native-like conditions. The ease of use, stability, and the range of tools that can be applied to tethered membrane systems will be highly beneficial to study membrane processes in isolation from the complex environment of the cellular membrane. We also show that more sophisticated analysis methods may be required to interpret neutron and electrochemical data of more complex protein-containing sparsely tethered membrane systems.

ASSOCIATED CONTENT

Supporting Information

The Supporting Information is available free of charge at https://pubs.acs.org/doi/10.1021/acs.jpcb.2c07252.

Figures S1–S4 and Tables S1–S3 (PDF)

AUTHOR INFORMATION

Corresponding Authors

Philipp A. M. Schmidpeter – *Weill Cornell Medicine, Department of Anesthesiology, New York, New York 10065, United States;* orcid.org/0000-0003-2871-9706; Email: pas2039@med.cornell.edu

Wolfgang Knoll – *Austrian Institute of Technology GmbH, 1210 Vienna, Austria; Danube Private University, 3500 Krems an der Donau, Austria;* orcid.org/0000-0003-1543-4090; Email: wolfgang.knoll@ait.ac.at

Authors

Jakob Andersson – *Austrian Institute of Technology GmbH, 1210 Vienna, Austria;* orcid.org/0000-0002-3675-1493

David Kleinheinz – *Austrian Institute of Technology GmbH, 1210 Vienna, Austria*

Ulrich Ramach – *Technische Universität Wien, 1040 Wien, Austria; CEST Kompetenzzentrum für Oberflächentechnologie, 2700 Wiener Neustadt, Austria;* orcid.org/0000-0002-1111-2994

Nikolaus Kiesenhofer – *Austrian Institute of Technology GmbH, 1210 Vienna, Austria*

Alex Ashenden – *Flinders University of South Australia, 5042 Adelaide, Australia*

https://doi.org/10.1021/acs.jpcb.2c07252
J. Phys. Chem. B 2023, 127, 3641–3650

Markus Valtiner − *Technische Universität Wien, 1040 Wien, Austria; CEST Kompetenzzentrum für Oberflächentechnologie, 2700 Wiener Neustadt, Austria;* orcid.org/0000-0001-5410-1067

Stephen Holt − *Australian Nuclear Science and Technology Organization, Lucas Heights, NSW 2234, Australia;* orcid.org/0000-0003-3189-8047

Ingo Koeper − *Flinders University of South Australia, 5042 Adelaide, Australia;* orcid.org/0000-0002-5933-6495

Complete contact information is available at: https://pubs.acs.org/10.1021/acs.jpcb.2c07252

Author Contributions

□These authors contributed equally to this work.

Notes

The authors declare no competing financial interest.

■ ACKNOWLEDGMENTS

The authors would like to acknowledge Prof. Crina Nimigean at Weill Cornell Medicine for facilitating the collaboration between our laboratories. J.A. was funded by Grant LSC19-026 by the Gesellschaft für Forschungsförderung Niederösterreich m.b.H. Philipp Schmidpeter received funding from the American Heart Association (18POST33960309). Neutron scattering experiments were funded by the Australian Nuclear Science and Technology Organization (Proposal Number P7878). The authors also acknowledge the European Research Council (ERC-StG 663677).

■ REFERENCES

(1) Overington, J. P.; Al-Lazikani, B.; Hopkins, A. L. How many drug targets are there? *Nat. Rev. Drug Discovery* **2006**, *5*, 993−996.
(2) Wei, F.; et al. Ion channel genes and epilepsy: functional alteration, pathogenic potential, and mechanism of epilepsy. *Neurosci. Bull.* **2017**, *33*, 455−477.
(3) DiFrancesco, J. C.; DiFrancesco, D. Dysfunctional HCN ion channels in neurological diseases. *Front. Cell. Neurosci.* **2015**, *6*, 10.
(4) Kunzelmann, K. Ion channels and cancer. *J. Membr. Biol.* **2005**, *205*, 159.
(5) Bates, E. Ion channels in development and cancer. *Annu. Rev. Cell Dev. Biol.* **2015**, *31*, 231−247.
(6) Hover, S.; Foster, B.; Barr, J. N.; Mankouri, J. Viral dependence on cellular ion channels−an emerging anti-viral target? *J. Gen. Virol.* **2017**, *98*, 345−351.
(7) Winterhalter, M. Black lipid membranes. *Curr. Opin. Colloid Interface Sci.* **2000**, *5*, 250−255.
(8) Andersson, J.; Köper, I.; Knoll, W. Tethered Membrane Architectures—Design and Applications. *Frontiers in Materials* **2018**, *5*, 55.
(9) Lin, W.; Yu, C.; Triffo, S.; Groves, J. T. Supported membrane formation, characterization, functionalization, and patterning for application in biological science and technology. *Curr. Protoc. Chem. Biol.* **2010**, *2*, 235−269.
(10) Benz, M.; Gutsmann, T.; Chen, N.; Tadmor, R.; Israelachvili, J. Correlation of AFM and SFA measurements concerning the stability of supported lipid bilayers. *Biophys. J.* **2004**, *86*, 870−879.
(11) Castellana, E. T.; Cremer, P. S. Solid supported lipid bilayers: From biophysical studies to sensor design. *Surf. Sci. Rep.* **2006**, *61*, 429−444.
(12) Vockenroth, I. K.; et al. Stable insulating tethered bilayer lipid membranes. *Biointerphases* **2008**, *3*, FA68−FA73.
(13) Vockenroth, I. K.; Fine, D.; Dodobalapur, A.; Jenkins, A. T. A.; Köper, I. Tethered bilayer lipid membranes with giga-ohm resistances. *Electrochem. commun.* **2008**, *10*, 323−328.
(14) Junghans, A.; Koper, I. Structural Analysis of Tethered Bilayer Lipid Membranes. *Langmuir* **2010**, *26*, 11035−11040.
(15) Vockenroth, I. K.; et al. Functional incorporation of the pore forming segment of AChR M2 into tethered bilayer lipid membranes. *Biochim. Biophys. Acta-Biomembranes* **2007**, *1768*, 1114−1120.
(16) Cranfield, C. G.; et al. Transient potential gradients and impedance measures of tethered bilayer lipid membranes: Pore-forming peptide insertion and the effect of electroporation. *Biophys. J.* **2014**, *106*, 182−189.
(17) Vockenroth, I. K.; Atanasova, P. P.; Jenkins, A. T. A.; Koper, I. Incorporation of alpha-hemolysin in different tethered bilayer lipid membrane architectures. *Langmuir* **2008**, *24*, 496−502.
(18) Kozuch, J.; Steinem, C.; Hildebrandt, P.; Millo, D. Combined Electrochemistry and Surface-Enhanced Infrared Absorption Spectroscopy of Gramicidin A Incorporated into Tethered Bilayer Lipid Membranes. *Angew. Chemie Int. Ed.* **2012**, *51*, 8114−8117.
(19) Preta, G.; et al. Tethered bilayer membranes as a complementary tool for functional and structural studies: The pyolysin case. *Biochim. Biophys. Acta (BBA)-Biomembranes* **2016**, *1858*, 2070−2080.
(20) Andersson, J.; Knobloch, J. J.; Perkins, M. V.; Holt, S. A.; Köper, I. Synthesis and Characterization of Novel Anchorlipids for Tethered Bilayer Lipid Membranes. *Langmuir* **2017**, *33*, 4444−4451.
(21) Kleinheinz, D.; et al. Functional incorporation of the insect odorant receptor coreceptor in tethered lipid bilayer nanoarchitectures. *Biosens. Bioelectron.* **2022**, *203*, 114024.
(22) Goreham, R. V.; Thompson, V. C.; Samura, Y.; Gibson, C. T.; Shapter, J. G.; Koper, I. Interaction of silver nanoparticles with tethered bilayer lipid membranes. *Langmuir* **2015**, *31*, 5868−5874.
(23) Andersson, J.; Fuller, M. A.; Wood, K.; Holt, S. A.; Köper, I. A tethered bilayer lipid membrane that mimics microbial membranes. *Phys. Chem. Chem. Phys.* **2018**, *20*, 12958−12969.
(24) Andersson, J.; Fuller, M.; Ashenden, A.; Holt, S. A.; Köper, I. Increasing Antibiotic Susceptibility: The Use of Cationic Gold Nanoparticles in Gram-Negative Bacterial Membrane Models. *Langmuir* **2021**, *37*, 9735−9743.
(25) Schmidpeter, P. A. M.; Gao, X.; Uphadyay, V.; Rheinberger, J.; Nimigean, C. M. Ligand binding and activation properties of the purified bacterial cyclic nucleotide-gated channel SthK. *J. Gen. Physiol.* **2018**, *150*, 821−834.
(26) Kaupp, U. B.; Seifert, R. Cyclic nucleotide-gated ion channels. *Physiol. Rev.* **2002**, *82*, 769−824.
(27) Brams, M.; Kusch, J.; Spurny, R.; Benndorf, K.; Ulens, C. Family of prokaryote cyclic nucleotide-modulated ion channels. *Proc. Natl. Acad. Sci. U. S. A.* **2014**, *111*, 7855−7860.
(28) Morgan, J. L. W.; Evans, E. G. B.; Zagotta, W. N. Functional characterization and optimization of a bacterial cyclic nucleotide−gated channel. *J. Biol. Chem.* **2019**, *294*, 7503−7515.
(29) Evans, E. G. B.; Morgan, J. L. W.; DiMaio, F.; Zagotta, W. N.; Stoll, S. Allosteric conformational change of a cyclic nucleotide-gated ion channel revealed by DEER spectroscopy. *Proc. Natl. Acad. Sci. U. S. A.* **2020**, *117*, 10839−10847.
(30) Rheinberger, J.; Gao, X.; Schmidpeter, P. A. M.; Nimigean, C. M. Ligand discrimination and gating in cyclic nucleotide-gated ion channels from apo and partial agonist-bound cryo-EM structures. *Elife* **2018**, *7*, e39775.
(31) Schmidpeter, P. A. M.; Wu, D.; Rheinberger, J.; Riegelhaupt, P. M.; Tang, H.; Robinson, C. V.; Nimigean, C. M. Anionic lipids unlock the gates of select ion channels in the pacemaker family. *Nat. Struct. Mol. Biol.* **2022**, *29*, 1092.
(32) Vogel, N.; Zieleniecki, J.; Köper, I. As flat as it gets: ultrasmooth surfaces from template-stripping procedures. *Nanoscale* **2012**, *4*, 3820−3832.
(33) Vockenroth, I. K.; Rossi, C.; Shah, M. R.; Köper, I. Formation of tethered bilayer lipid membranes probed by various surface sensitive techniques. *Biointerphases* **2009**, *4*, 19−26.
(34) Kesters, D.; et al. Structure of the SthK carboxy-terminal region reveals a gating mechanism for cyclic nucleotide-modulated ion channels. *PLoS One* **2015**, *10*, e0116369.

(35) Marchesi, A.; Gao, X.; Adaixo, R.; Rheinberger, J.; Stahlberg, H.; Nimigean, C.; Scheuring, S. An iris diaphragm mechanism to gate a cyclic nucleotide-gated ion channel. *Nat. Commun.* **2018**, *9*, 1−11.
(36) Nelson, A. R. J.; Prescott, S. W. Refnx: Neutron and X-ray reflectometry analysis in python. *J. Appl. Crystallogr.* **2019**, *52*, 193−200.
(37) Shekhar, P.; Nanda, H.; Lösche, M.; Heinrich, F. Continuous distribution model for the investigation of complex molecular architectures near interfaces with scattering techniques. *J. Appl. Phys.* **2011**, *110*, 102216.
(38) Efimova, Y. M.; Van Well, A. A.; Hanefeld, U.; Wierczinski, B.; Bouwman, W. G. On the neutron scattering length density of proteins in H2O/D2O. *Phys. B Condens. Matter* **2004**, *350*, E877−E880.
(39) Hoogerheide, D. P.; et al. Structure of voltage-dependent anion channel-tethered bilayer lipid membranes determined using neutron reflectivity. *Acta Crystallogr. Sect. D Struct. Biol.* **2018**, *74*, 1219−1232.
(40) Valincius, G.; Meskauskas, T.; Ivanauskas, F. Electrochemical Impedance Spectroscopy of Tethered Bilayer Membranes. *Langmuir* **2012**, *28*, 977−990.
(41) Budvytyte, R.; et al. Structure and Properties of Tethered Bilayer Lipid Membranes with Unsaturated Anchor Molecules. *Langmuir* **2013**, *29*, 8645−8656.
(42) Schiller, S. M.; Naumann, R.; Lovejoy, K.; Kunz, H.; Knoll, W. Archaea analogue thiolipids for tethered bilayer lipid membranes on ultrasmooth gold surfaces. *Angew. Chemie Int. Ed.* **2003**, *42*, 208−211.
(43) Naumann, R.; et al. The peptide-tethered lipid membrane as a biomimetic system to incorporate cytochrome c oxidase in a functionally active form. *Biosens. Bioelectron.* **1999**, *14*, 651−662.
(44) Hoomann, T.; Jahnke, N.; Horner, A.; Keller, S.; Pohl, P. Filter gate closure inhibits ion but not water transport through potassium channels. *Proc. Natl. Acad. Sci. U. S. A.* **2013**, *110*, 10842−10847.
(45) Gramse, G.; Dols-Pérez, A.; Edwards, M. A.; Fumagalli, L.; Gomila, G. Nanoscale measurement of the dielectric constant of supported lipid bilayers in aqueous solutions with electrostatic force microscopy. *Biophys. J.* **2013**, *104*, 1257−1262.
(46) Ng, J. A.; Vora, T.; Krishnamurthy, V.; Chung, S.-H. Estimating the dielectric constant of the channel protein and pore. *Eur. Biophys. J.* **2008**, *37*, 213−222.
(47) Aoki, K. J. Frequency-dependence of electric double layer capacitance without Faradaic reactions. *J. Electroanal. Chem.* **2016**, *779*, 117−125.
(48) Awayda, M. S.; Van Driessche, W.; Helman, S. I. Frequency-dependent capacitance of the apical membrane of frog skin: dielectric relaxation processes. *Biophys. J.* **1999**, *76*, 219−232.
(49) McGillivray, D. J.; et al. Molecular-scale structural and functional characterization of sparsely tethered bilayer lipid membranes. *Biointerphases* **2007**, *2*, 21−33.
(50) Khan, M. S.; Dosoky, N. S.; Berdiev, B. K.; Williams, J. D. Electrochemical impedance spectroscopy for black lipid membranes fused with channel protein supported on solid-state nanopore. *Eur. Biophys. J.* **2016**, *45*, 843−852.
(51) Su, Z.; et al. EIS and PM-IRRAS studies of alamethicin ion channels in a tethered lipid bilayer. *J. Electroanal. Chem.* **2018**, *812*, 213−220.
(52) Raila, T.; et al. Electrochemical impedance of randomly distributed defects in tethered phospholipid bilayers: Finite element analysis. *Electrochim. Acta* **2019**, *299*, 863−874.
(53) Schmidpeter, P. A. M.; Nimigean, C. M. Correlating ion channel structure and function. *Methods in Enzymology* **2021**, *652*, 3−30.
(54) Wirth, R.; Ugele, M.; Wanner, G. Motility and Ultrastructure of Spirochaeta thermophila. *Front. Microbiol.* **2016**, *7*, 1609.

https://doi.org/10.1021/acs.jpcb.2c07252
J. Phys. Chem. B 2023, 127, 3641−3650